S-1. Identified compounds from UHPLC–(-)ESI–UHRMS analysis of filter samples

Table S-1: List of CHO-containing compounds that were identified by UHPLC–(-)ESI–UHRMS analysis of the filter samples.

formula for $[M–H]^−$	*m/z* for $[M–H]^−$	measured *m/z*	Δ*m* / ppm	Number of Oxygen	Number of Carbon	O:C
$C_4H_5O_5$	133.0142	133.0141	-1.1	5	4	1.3
$C_6H_7O_4$	143.0350	143.0349	-0.6	4	6	0.7
$C_6H_9O_4$	145.0506	145.0506	-0.2	4	6	0.7
$C_6H_9O_5$	161.0455	161.0454	-0.9	5	6	0.8
$C_6H_{13}O_6$	181.0718	181.0718	0.2	6	6	1.0
$C_6H_7O_7$	191.0197	191.0197	-0.1	7	6	1.2
$C_7H_9O_3$	141.0557	141.0557	-0.1	3	7	0.4
$C_7H_9O_4$	157.0506	157.0505	-0.9	4	7	0.6
$C_7H_{11}O_4$	159.0663	159.0661	-1.2	4	7	0.6
$C_7H_9O_5$	173.0455	173.0453	-1.4	5	7	0.7
$C_7H_{11}O_5$	175.0612	175.0611	-0.6	5	7	0.7
$C_7H_7O_6$	187.0248	187.0247	-0.6	6	7	0.9
$C_7H_9O_6$	189.0405	189.0403	-0.9	6	7	0.9
$C_8H_{13}O_3$	157.0870	157.0871	0.5	3	8	0.4
$C_8H_{11}O_4$	171.0663	171.0662	-0.5	4	8	0.5
$C_8H_{11}O_5$	187.0612	187.061	-1.1	5	8	0.6
$C_8H_{13}O_5$*	189.0768	189.0767	-0.8	5	8	0.6
$C_8H_9O_6$	201.0405	201.0403	-0.8	6	8	0.8
$C_8H_{11}O_6$*	203.0561	203.0561	-0.1	6	8	0.8
$C_9H_7O_4$	179.0350	179.0351	0.7	4	9	0.4
$C_9H_{13}O_4$	185.0819	185.0818	-0.7	4	9	0.4
$C_9H_{11}O_5$	199.0612	199.0612	0.0	5	9	0.6
$C_9H_{13}O_5$	201.0768	201.0768	-0.2	5	9	0.6
$C_9H_{15}O_5$	203.0925	203.0925	0.0	5	9	0.6
$C_9H_9O_6$	213.0405	213.0405	0.2	6	9	0.7
$C_9H_{11}O_6$	215.0561	215.0555	-2.9	6	9	0.7
$C_9H_{13}O_6$	217.0718	217.0716	-0.8	6	9	0.7
$C_9H_9O_7$	229.0354	229.0348	-2.5	7	9	0.8
$C_9H_{11}O_7$	231.0510	231.0505	-2.3	7	9	0.8
$C_{10}H_{15}O_3$	183.1027	183.1026	-0.4	3	10	0.3
$C_{10}H_{13}O_5$	213.0768	213.0768	-0.2	5	10	0.5
$C_{10}H_{15}O_5$	215.0925	215.0924	-0.5	5	10	0.5
$C_{10}H_{13}O_6$	229.0718	229.0715	-1.2	6	10	0.6

$C_{10}H_{15}O_6$	231.0874	231.0872	-0.9	6	10	0.6
$C_{10}H_{11}O_7$	243.0510	243.0506	-1.8	7	10	0.7
$C_{10}H_{15}O_7$	247.0823	247.0822	-0.5	7	10	0.7
$C_{11}H_{15}O_6$	243.0874	243.0873	-0.5	6	11	0.5
$C_{11}H_{17}O_6$*	245.1031	245.103	-0.3	6	11	0.5
$C_{12}H_{19}O_5$	243.1238	243.1237	-0.4	5	12	0.4
$C_{12}H_{21}O_5$	245.1394	245.1392	-1.0	5	12	0.4
$C_{13}H_{19}O_5$	255.1238	255.1239	0.4	5	13	0.4
$C_{13}H_{19}O_6$	271.1187	271.1188	0.3	6	13	0.5
$C_{14}H_{21}O_5$*	269.1394	269.1394	-0.2	5	14	0.4
$C_{17}H_{25}O_8$	357.1555	357.1559	1.1	8	17	0.5

*isobaric compounds detected

Table S-2: List of CHONS-containing compounds that were identified by UHPLC–(-)ESI–UHRMS analysis of the filter samples.

formula for [M–H]⁻	***m/z* for [M–H]⁻**	**measured *m/z***	**Δ*m* / ppm**	**Number of Oxygen**	**Number of Carbon**	**O:C**
$C_5H_{10}O_9NS$	260.0082	260.0079	-1.1	9	5	1.8
$C_5H_9O_{11}N_2S$	304.9933	304.9932	-0.2	11	5	2.2
$C_6H_{10}O_9NS$	272.0082	272.0081	-0.3	9	6	1.5
$C_7H_{10}O_9NS$	284.0082	284.0080	-0.6	9	7	1.3
$C_7H_{10}O_{10}NS$	300.0031	300.0029	-0.6	10	7	1.4
$C_{10}H_{16}O_7NS$	294.0653	294.0657	1.4	7	10	0.7
$C_{10}H_{14}O_8NS$	308.0446	308.0448	0.8	8	10	0.8
$C_{10}H_{16}O_8NS$	310.0602	310.0605	0.9	8	10	0.8
$C_{10}H_{16}O_9NS$	326.0551	326.0551	-0.1	9	10	0.9
$C_{10}H_{16}O_{10}NS$	342.0500	342.0497	-1.0	10	10	1.0
$C_{10}H_{18}O_{10}NS$	344.0657	344.0655	-0.6	10	10	1.0
$C_{10}H_{17}O_{11}$N2S	373.0559	373.0558	-0.2	11	10	1.1
$C_{10}H_{15}O_{12}N_2S$	387.0351	387.0350	-0.3	12	10	1.2

Table S-3: List of CHON-containing compounds that were identified by UHPLC–(-)ESI–UHRMS analysis of the filter samples.

formula for [M–H]⁻	***m/z* for [M–H]⁻**	**measured *m/z***	**Δ*m* / ppm**	**Number of Oxygen**	**Number of Carbon**	**O:C**
$C_7H_4O_5N$	182.0095	182.0096	0.6	5	7	0.7
$C_7H_3O_7N_2$	226.9946	226.9947	0.5	7	7	1.0
$C_{10}H_{16}O_8N$	278.0881	278.0882	0.2	8	10	0.8
$C_{11}H_{18}O_9N$	308.0987	308.0988	0.3	9	11	0.8

Table S-4: List of CHOS-containing compounds that were identified by UHPLC–(-)ESI–UHRMS analysis of the filter samples.

formula for $[M–H]^-$	*m/z* for $[M–H]^-$	measured *m/z*	Δ*m* / ppm	Number of Oxygen	Number of Carbon	O:C
$C_2H_3O_6S$	154.9656	154.9656	0.1	6	2	3.0
$C_3H_5O_6S$	168.9812	168.9812	-0.2	6	3	2.0
$C_4H_7O_6S$	182.9969	182.9967	-1.0	6	4	1.5
$C_5H_9O_6S$	197.0125	197.0124	-0.7	6	5	1.2
$C_5H_{11}O_6S$	199.0282	199.0280	-0.9	6	5	1.2
$C_5H_7O_7S$	210.9918	210.9916	-0.9	7	5	1.4
$C_5H_9O_7S$	213.0074	213.0075	0.2	7	5	1.4
$C_5H_{11}O_7S$	215.0231	215.0229	-0.9	7	5	1.4
$C_5H_7O_8S$	226.9867	226.9865	-0.9	8	5	1.6
$C_6H_{11}O_6S$	211.0282	211.0280	-0.9	6	6	1.0
$C_7H_{11}O_6S$	223.0282	223.0280	-0.8	6	7	0.9
$C_7H_{11}O_7S$	239.0231	239.0231	0.0	7	7	1.0
$C_7H_{13}O_7S$	241.0387	241.0385	-1.0	7	7	1.0
$C_7H_7O_8S$	250.9867	250.9868	0.3	8	7	1.1
$C_7H_9O_8S$	253.0024	253.0028	1.7	8	7	1.1
$C_8H_{13}O_7S$	253.0387	253.0384	-1.4	7	8	0.9
$C_8H_{11}O_9S$	283.0129	283.0127	-0.8	9	8	1.1
$C_8H_{13}O_9S$	285.0286	285.0284	-0.6	9	8	1.1
$C_8H_{13}O_{10}S$	301.0235	301.0231	-1.3	10	8	1.3
$C_9H_{15}O_6S$	251.0595	251.0593	-0.7	6	9	0.7
$C_9H_{15}O_7S$	267.0544	267.0540	-1.5	7	9	0.8
$C_9H_{13}O_8S$	281.0337	281.0334	-0.9	8	9	0.9
$C_9H_{13}O_9S$	297.0286	297.0282	-1.3	9	9	1.0
$C_{10}H_{17}O_5S$	249.0802	249.0801	-0.5	5	10	0.5
$C_{10}H_{15}O_7S$	279.0544	279.0544	0.0	7	10	0.7
$C_{10}H_{17}O_7S$	281.0700	281.0698	-0.9	7	10	0.7
$C_{10}H_{17}O_8S$	297.0650	297.0646	-1.2	8	10	0.8
$C_{10}H_{15}O_9S$	311.0442	311.0440	-0.7	9	10	0.9
$C_{10}H_{17}O_9S$	313.0599	313.0596	-0.9	9	10	0.9
$C_{10}H_{15}O_{10}S$	327.0391	327.0387	-1.4	10	10	1.0
$C_{10}H_{13}O_{11}S$	341.0184	341.0183	-0.3	11	10	1.1
$C_{11}H_{19}O_7S$	295.0857	295.0858	0.3	7	11	0.6

S-2. Trajectory calculations for the campaign period

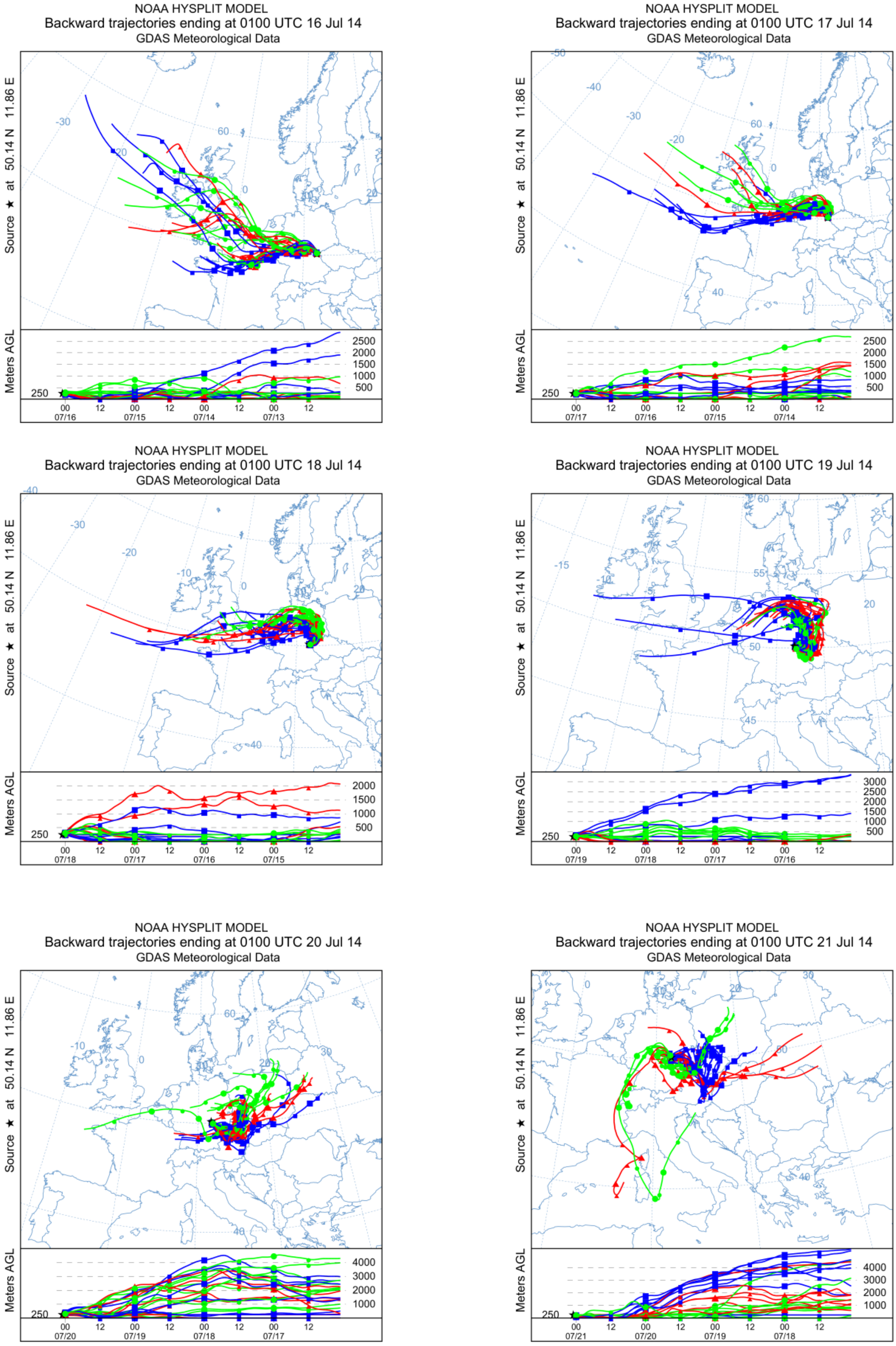

Figure S-1: 96 hours backward HYSPLIT trajectory calculations for the 16th-21st of July (each at 12 midnight CET) (Draxler and Rolph).

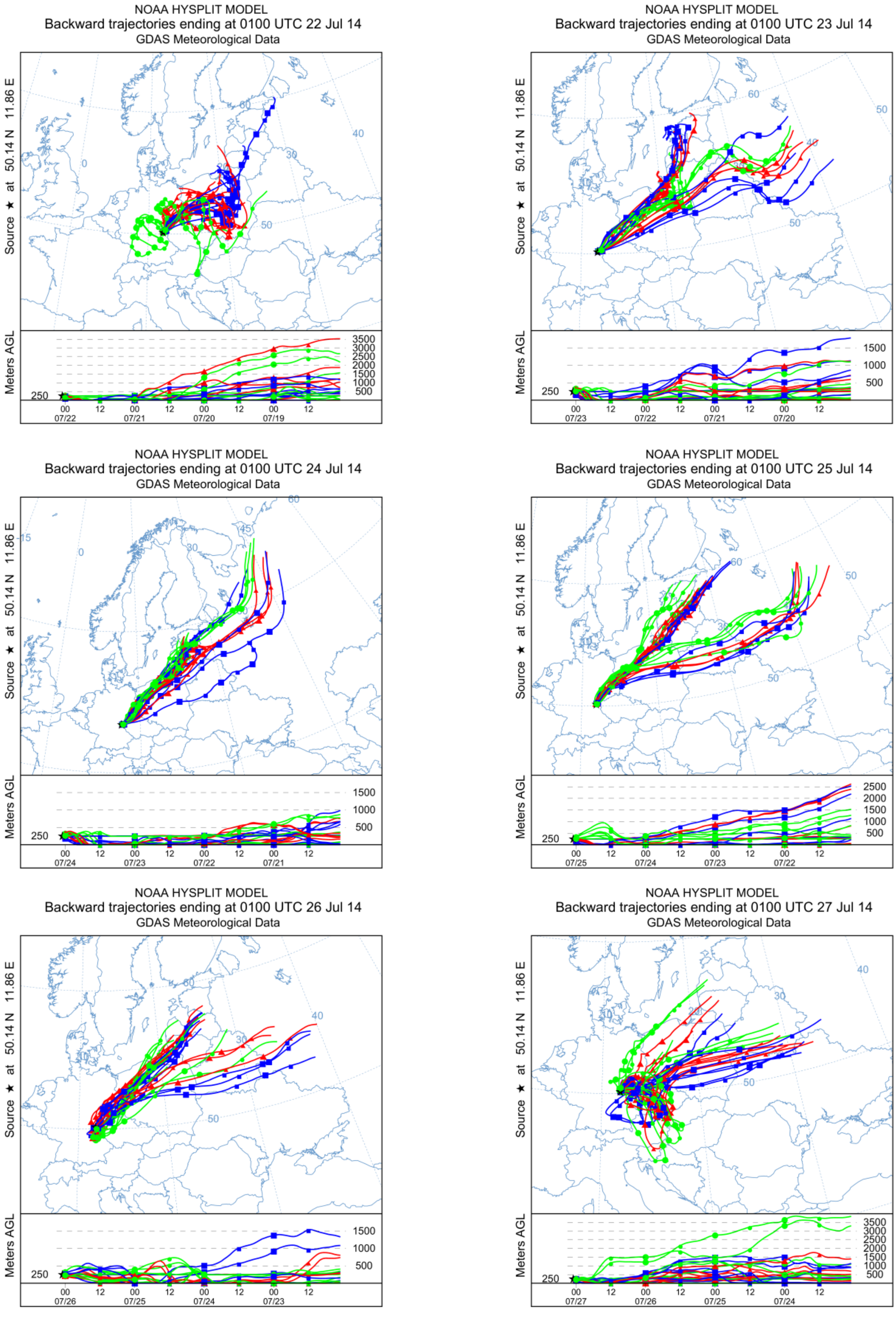

Figure S-2: 96 hours backward HYSPLIT trajectory calculations for the 22nd–27th of July (each at 12 midnight CET) (Draxler and Rolph).

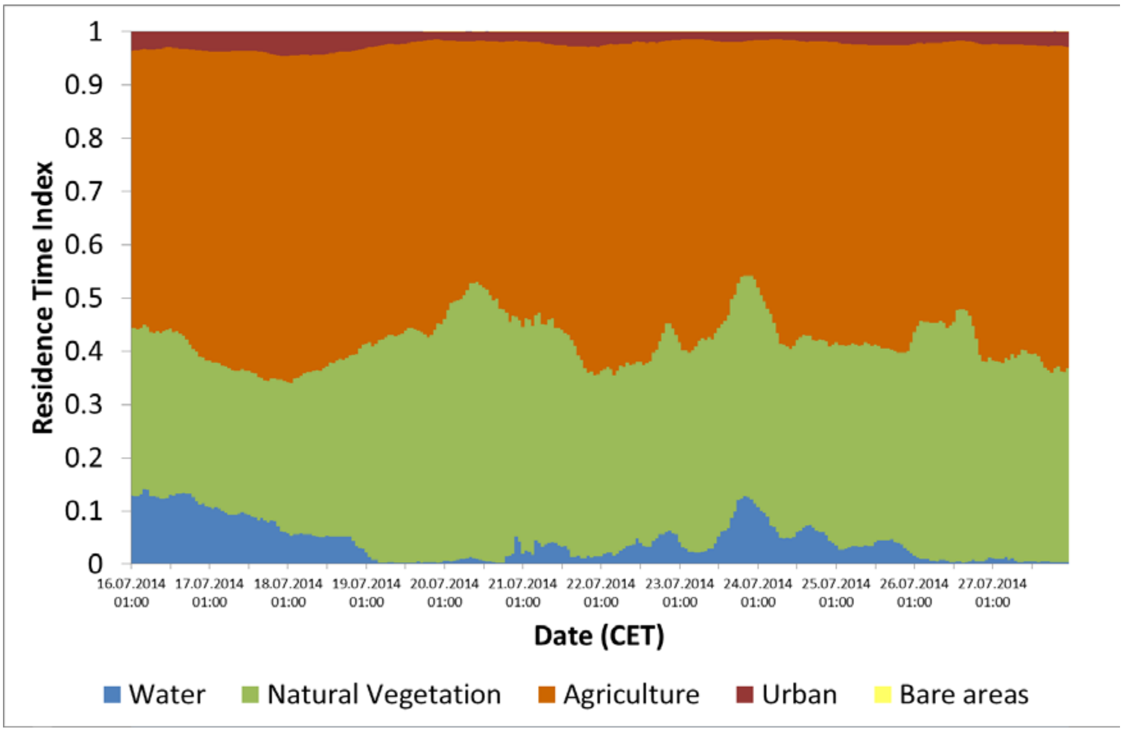

Figure S-3: Residence times for 96 hours backward trajectories arriving at the site intersected with satellite-derived global landcover data to give indications of influences of main land cover classes. A detailed description of the calculation method can be found elsewhere (van Pinxteren et al., 2010).

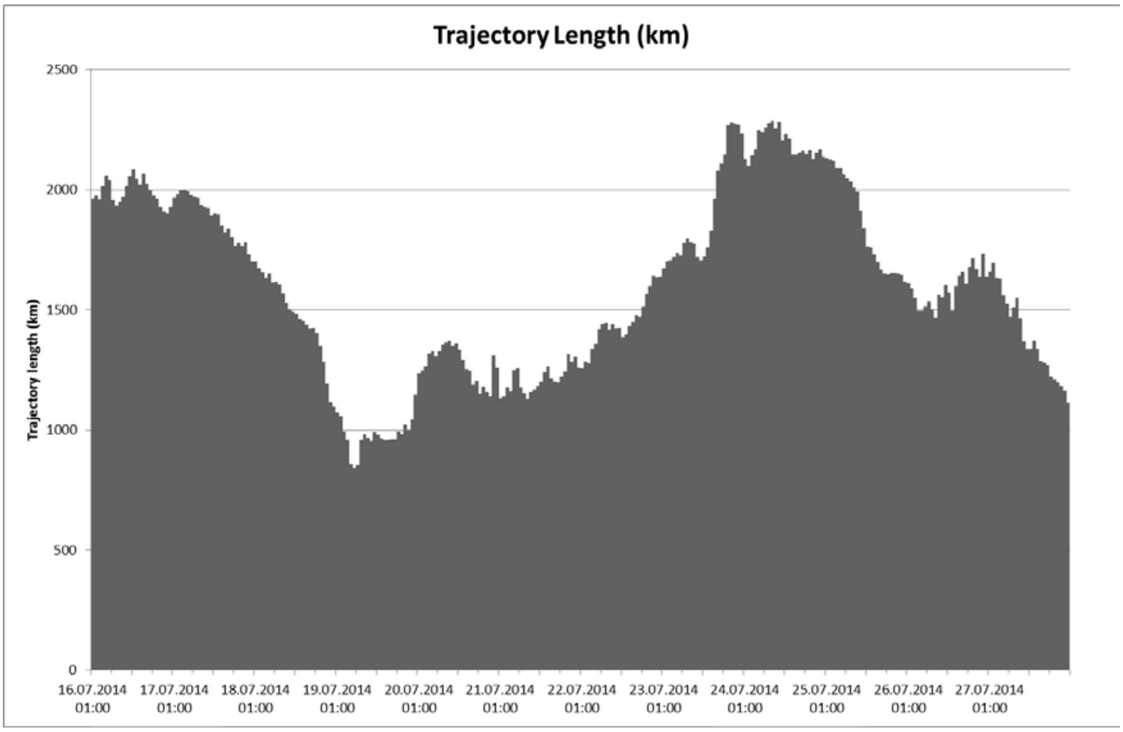

Figure S-4: Trajectory lengths for 96 hours backward trajectories arriving at the site. For details see van Pinxteren et al. (2010).

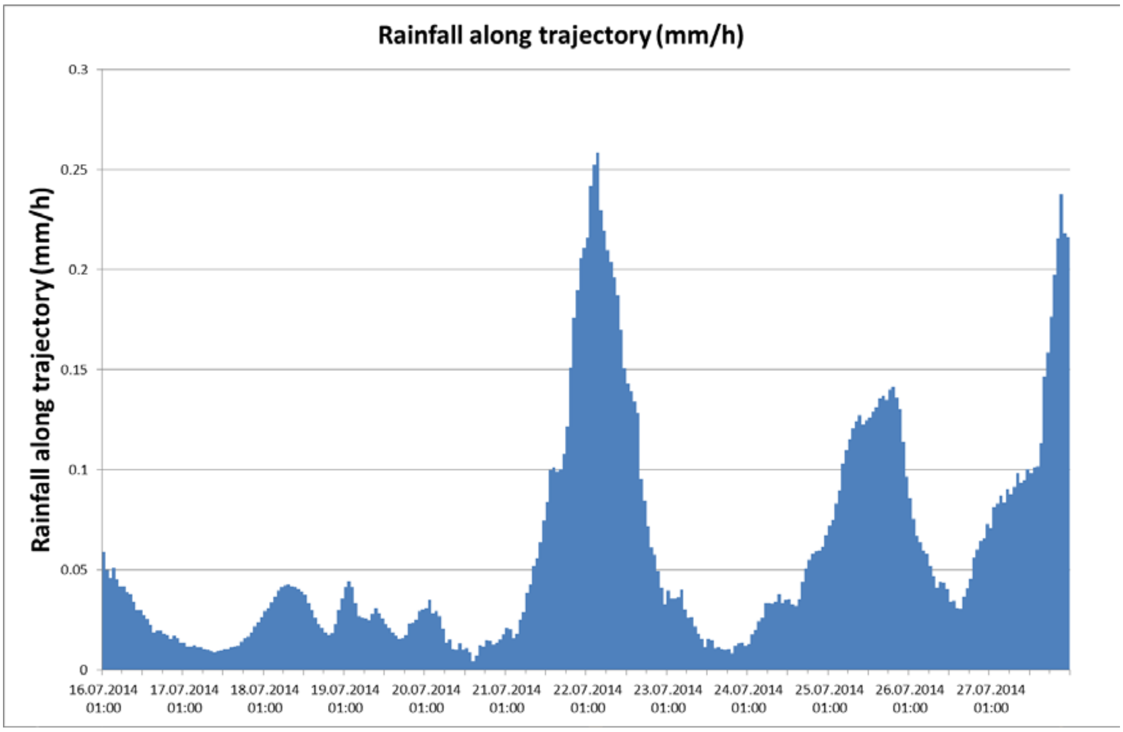

Figure S-5: Rainfall along the calculated 96 hours backward trajectories arriving at the site. For details see van Pinxteren et al. (2010).

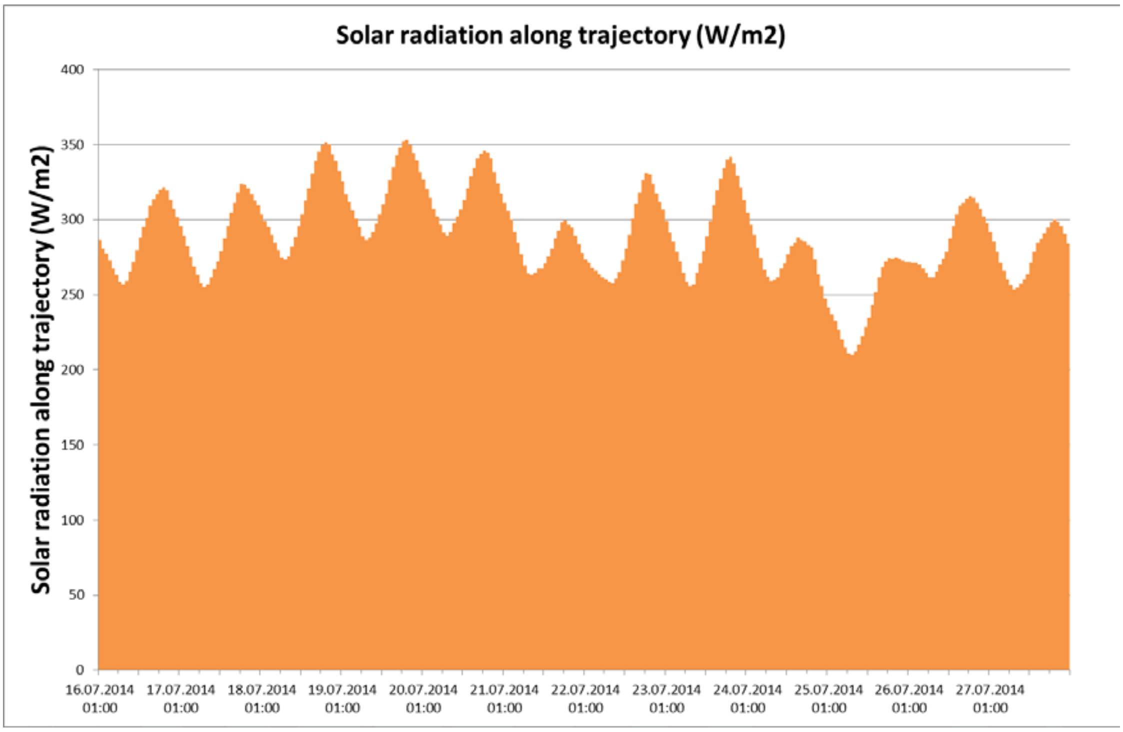

Figure S-6: Solar radiation along the calculated 96 hours backward trajectories arriving at the site. For details see van Pinxteren et al. (2010).

S-3. Supplementary mass spectrometric data

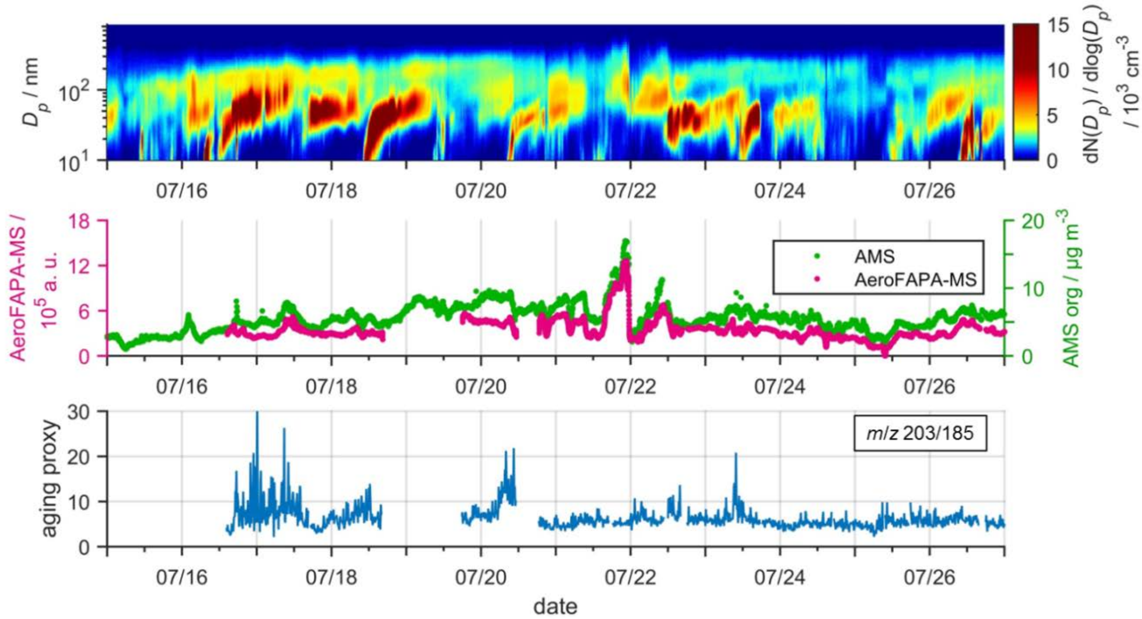

Figure S-7: Top panel: Number size distribution of aerosol particles which was measured by an SMPS. Middle panel: Time traces of the total ion current of the AeroFAPA–MS (magenta) and the organic aerosol mass measured by an AMS (green). Bottom panel: Ratio of *m*/*z* 203/185 as aging proxy for SOA particles at the site.

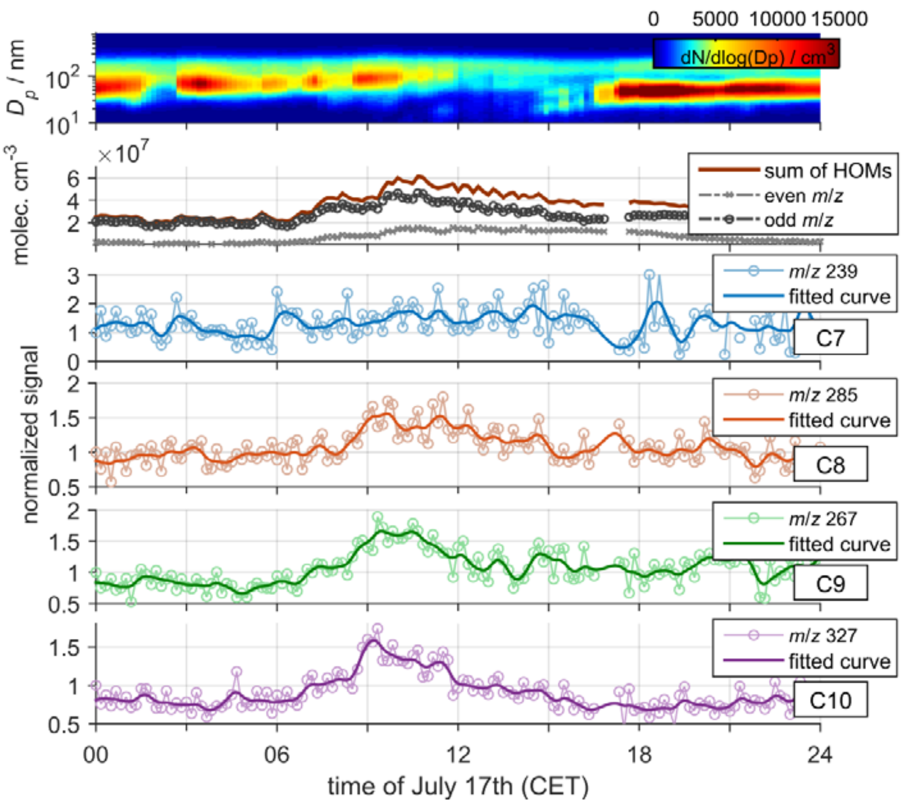

Figure S-8: Time traces for C7–C10 HOOS, gas-phase HOMs and particle number size distribution during July 17th. HOM concentration is dominated by ions with odd *m*/*z* ratios ($[M+NO_3]^-$), indicating the presence of peroxyradicals ($RO_2^{\bullet}$), organonitrates ($RONO_2$) and peroxynitrates (RO_2NO_2). While the larger HOOS are following the trend of the HOM signals with odd *m*/*z* ratios, the C7 HOOS differ from this behavior, supporting the assumption that these species are not directly formed but by decomposition of the larger HOOS.

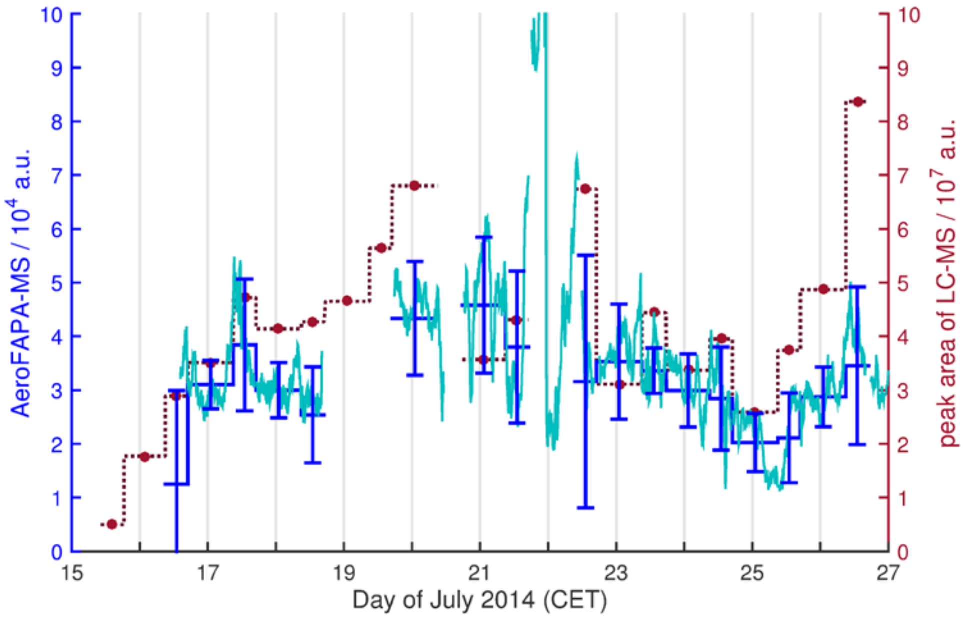

Figure S-9: Comparison of the signals for the sum of HOOS detected by AeroFAPA–MS (light blue), and by LC–MS (red). The signals of the AeroFAPA–MS are averaged for the filter sampling times (dark blue); error bars depict one standard deviation.

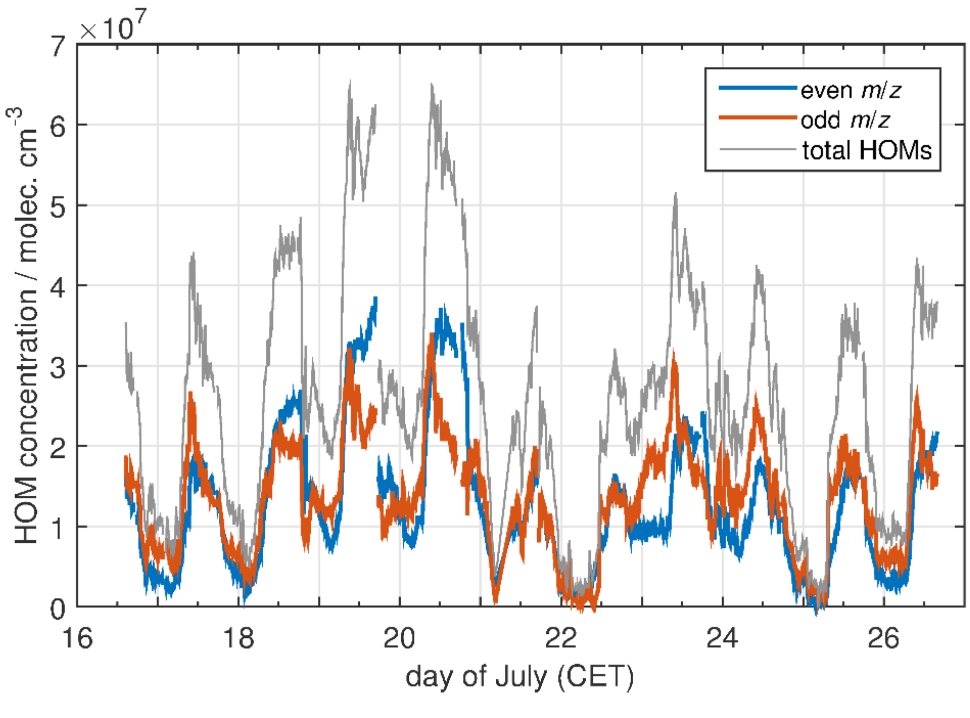

Figure S-10: Concentrations of gas-phase HOMs measured by the CI–APiToF–MS over the entire campaign period.

Table S-5: Signals and assignments for gas-phase HOMs detected by CI–APiTOF–MS.

formula assignment	**classification**	**molecular weight**	***m/z* for $[M+NO_3]^-$**	**reference**
$C_7H_{10}O_4$	HOM	158	220	Ehn *et al.*, 2014
$C_{10}H_{15}O_6$	RO_2 radical	231	293	Jokinen *et al.*, 2014
–	–	232	294	
–	–	233	295	
–	–	235	297	
$C_8H_{12}O_8$	HOM	236	298	Ehn *et al.*, 2014
–	–	245	307	
$C_{10}H_{14}O_7$	HOM	246	308	Ehn *et al.*, 2014
–	–	247	309	
$C_9H_{12}O_8$ / $C_{10}H_{16}O_7$	HOM	248	310	Ehn *et al.*, 2014
$C_{10}H_{17}O_7$	RO_2 radical	249	311	Jokinen *et al.*, 2014
$C_{10}H_{15}O_8$	RO_2 radical	263	325	Jokinen *et al.*, 2014
$C_{10}H_{16}O_8$ / $C_9H_{12}O_9$	HOM	264	326	Ehn *et al.*, 2014
–	–	265	327	
–	–	267	329	
–	RO_2NO_2 (*m/z* 293+NO_2)	277	339	Jokinen *et al.*, 2014
$C_{10}H_{14}O_9$	HOM	278	340	Ehn *et al.*, 2014
$C_{10}H_{16}O_9$	HOM	280	342	Ehn *et al.*, 2014
–	$RONO_2$ (*m/z* 325+NO)	293	355	Jokinen *et al.*, 2014
$C_{10}H_{15}O_{10}$	RO_2 radical	295	357	Jokinen *et al.*, 2014
$C_{10}H_{16}O_{10}$	HOM	296	358	Ehn *et al.*, 2014
–	–	308	370	
$C_{10}H_{14}O_{11}$	HOM	310	372	Ehn *et al.*, 2014
$C_{10}H_{16}O_{11}$	HOM	312	374	Ehn *et al.*, 2014

References

Draxler, R. and Rolph, G.: HYSPLIT (HYbrid Single-Particle Lagrangian Integrated Trajectory) Model.

Ehn, M., Thornton, J. A., Kleist, E., Sipila, M., Junninen, H., Pullinen, I., Springer, M., Rubach, F., Tillmann, R., Lee, B., Lopez-Hilfiker, F., Andres, S., Acir, I.-H., Rissanen, M., Jokinen, T., Schobesberger, S., Kangasluoma, J., Kontkanen, J., Nieminen, T., Kurten, T., Nielsen, L. B., Jorgensen, S., Kjaergaard, H. G., Canagaratna, M., Maso, M. D., Berndt, T., Petaja, T., Wahner, A., Kerminen, V.-M., Kulmala, M., Worsnop, D. R., Wildt, J., and Mentel, T. F.: A large source of low-volatility secondary organic aerosol, Nature, 506, 476–479, 2014.

Jokinen, T., Sipilä, M., Richters, S., Kerminen, V.-M., Paasonen, P., Stratmann, F., Worsnop, D., Kulmala, M., Ehn, M., Herrmann, H., and Berndt, T.: Rapid Autoxidation Forms Highly Oxidized RO2 Radicals in the Atmosphere, Angew. Chem. Int. Ed., 53, 14596–14600, doi:10.1002/anie.201408566, 2014.

van Pinxteren, D., Brüggemann, E., Gnauk, T., Müller, K., Thiel, C., and Herrmann, H.: A GIS based approach to back trajectory analysis for the source apportionment of aerosol constituents and its first application, J Atmos Chem, 67, 1-28, doi:10.1007/s10874-011-9199-9, 2010.